

Highly Ordered Self-Assembly with Large Area of Fe₃O₄ Nanoparticles and the Magnetic Properties

Tianzhong Yang,[†] Chengmin Shen,[†] Zian Li,[†] Huairuo Zhang,[†] Congwen Xiao,[†] Shutang Chen,^{†,‡} Zhichuan Xu,^{†,‡} Dongxia Shi,[†] Jianqi Li,[†] and Hongjun Gao^{*,†}

Institute of Physics, Chinese Academy of Sciences, Beijing 100080, China, and College of Chemistry and Chemical Engineering, Lanzhou University, Lanzhou 730000, China

Received: August 3, 2005; In Final Form: October 15, 2005

Monodisperse Fe₃O₄ nanoparticles (NPs) with narrow size distribution are synthesized by a high-temperature solution-phase method. The diameter of the as-synthesized NPs is tuned from 2 to 14 nm by varying the reaction conditions. Highly ordered superlattice structures of the Fe₃O₄ NPs with areas extending over 0.8 $\mu\text{m} \times 0.7 \mu\text{m}$ have been successfully obtained. The magnetic properties are investigated in their different states, such as in the solid state and diluted in wax with different concentrations. Some magnetic properties enhanced by increasing interparticle distances, such as the remanent magnetization and coercive field at low temperature, were noticed. Furthermore, we also observed that the saturation magnetization changed with temperature as expected. The preliminary explanation for the properties mentioned above is proposed.

Introduction

Materials at the nanometer scale have been studied for decades because of their unique properties arising from the large fraction of atoms residing on the surface, and also from the finite number of atoms in each crystalline core.^{1–8} Among these materials, superparamagnetic iron oxide nanoparticles (SPION) with suitable biocompatible coatings have been used in biomedicine, particularly in magnetic resonance imaging (MRI), tissue engineering, and drug delivery applications. Especially, because of the increasing need for high area density storage, the synthesis and characterization of magnetic nanoparticles have been extensively investigated.^{9–13} Metal and semiconductor nanocrystal dispersions exhibiting extremely narrow size distributions are thought to be a prerequisite for electronic and optical device applications. On the other hand, the assembly of uniform nanoparticles into well-defined two- and three-dimensional superlattices has attracted much attention, because it is critically important to chemical, optical, magnetic, and electronic nanodevices and would bring possibilities to brand-new properties and applications which result from the spatial orientation and arrangement of the nanocrystals.^{14–16} Here, we report on the synthesis of monodisperse Fe₃O₄ nanoparticles with narrow size distribution, monolayer and multilayer self-assemblies of the as-synthesized grains, and the magnetic properties of the NPs.

Experimental Section

Typically, we mixed Fe(acac)₃, 1,2-dodecanediol, oleic acid (OA), and oleylamine (the molar ratio is 2:5:3:3) in phenyl ether under the protection of nitrogen. Then, the mixture was heated to 200 °C. After maintaining the temperature for about 30 min, the mixture was heated to about 270 °C, and the temperature was maintained for 1 h. Then, it was cooled to room temperature naturally, and a large excess of ethanol was added under ambient

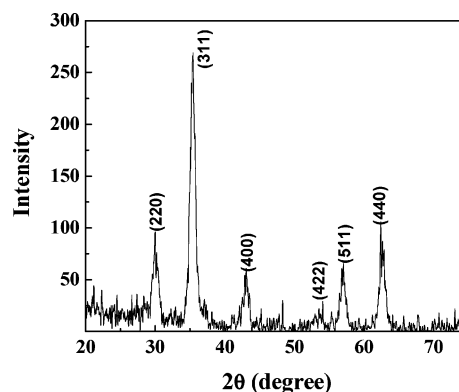


Figure 1. The XRD pattern of 8 nm Fe₃O₄ NPs, which shows the cubic spinel structure of the samples.

conditions. After centrifugation and purification, a black material was obtained and dissolved in heptane. The as-synthesized NPs with a diameter of about 4 nm are stable in heptane for at least 10 months and will be more stable with the presence of oleic acid and oleylamine. They can also be stable and redispersible in the solid state for some weeks after they are dried under ambient conditions. When the conditions were maintained at 270 °C for 2 h, the NP diameters were enlarged to about 8 nm. Higher initial precursor concentration leads to larger particles, but 14 nm is the limit to the NPs diameter by this way in our work. When lauric acid was used instead of oleic acid (OA) with the experimental parameters kept the same, the NPs became twice as large. We employed 1,2-dodecanediol with shorter carbon chains instead of 1,2-hexadecanediol to synthesize NPs, controlling particle sizes by varying the experimental conditions, which are different points from the method described in the literature.¹⁶

Results and Discussion

Figure 1 shows an XRD pattern of 8 nm Fe₃O₄ nanoparticles which indicates the highly crystalline cubic spinel structure. The

* E-mail: hjgao@aphy.iphy.ac.cn.

[†] Chinese Academy of Sciences.

[‡] Lanzhou University.

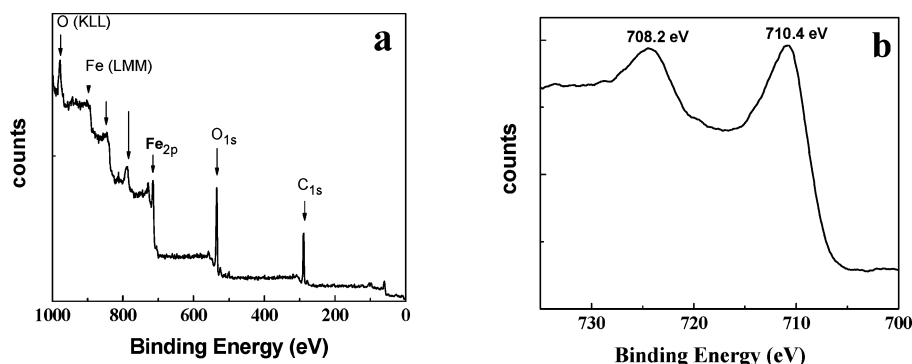


Figure 2. (a) XPS of the as-synthesized magnetite NPs. Evidence for the existence of the organic coating can be found. (b) The details of the iron Fe 2p_{1/2} and Fe 2p_{3/2} peaks, which match well with the standard data from the handbook.¹⁹

TABLE 1: Measured lattice spacing, $d(\text{\AA})$, based on the ED (Figure 3a)^a

	1	2	3	4	5	6	7	8	9	10
d	4.85	2.96	2.52	2.11	1.7	1.63	1.47	1.31	1.29	1.20
Fe ₃ O ₄	4.86	2.97	2.53	2.1	1.71	1.62	1.48	1.33	1.28	1.21
hkl	111	220	311	400	422	511	440	620	533	444

^a Standard atomic spacing for Fe₃O₄ along with their respective hkl indexes from the PDF database.¹⁶

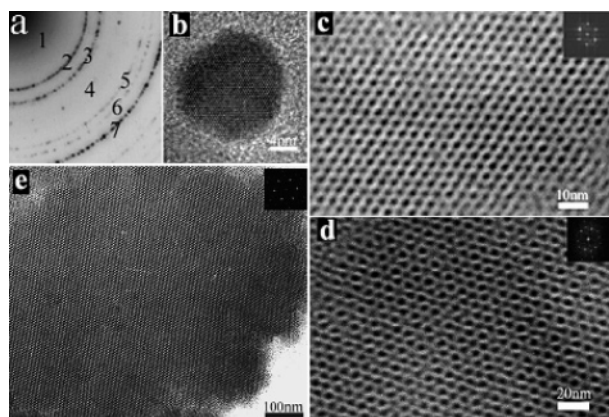


Figure 3. (a) ED patterns of the as-synthesized NPs. (b) HRTEM image of a single 14 nm Fe₃O₄ nanoparticle showing the detailed structure of the as-synthesized sample. (c) TEM image of magnetite NPs monolayer self-assembly. The inset is the FFT, which shows the structure of the monolayer. (d) TEM image of Fe₃O₄ NPs multilayer self-assembly. The FFT (inset) shows the NPs are arrayed in a hexagonal closed packed way. (e) Highly ordered superlattice with an area of about 0.8 $\mu\text{m} \times 0.7 \mu\text{m}$.

reflection peak positions and relative intensities of Fe₃O₄ nanoparticles agree well with those XRD patterns of Fe₃O₄ NPs in the literature,^{14–18} which confirms the structure of the magnetite materials. The average size of the Fe₃O₄ nanoparticles deduced from Sherrer's formula based on Figure 1 is about 8 nm, which is consistent with the result obtained from the transmission electron microscopy (TEM) analysis of the same sample, and the conclusion is that the particles are nearly single crystals.

X-ray photoelectron spectra of the Fe₃O₄ NPs are shown in Figure 2. The peaks of the C_{1s}, O_{2p}, N_{1s}, and Fe_{2p} observed in Figure 2a collectively indicate the organic coating on the surface of the Fe₃O₄ particles. Detail of the XPS (Figure 2b) shows binding energies of 708.2 and 710.4 eV, corresponding to Fe_{2p}_{3/2} and Fe_{2p}_{1/2}, respectively, in good agreement with the values reported for Fe₃O₄ in the handbook.¹⁹

The electron diffraction pattern of the Fe₃O₄ NPs exhibiting a magnetite structure is shown in Figure 3a. Table 1 shows the measured lattice spacing based on the rings in the electron diffraction pattern (Figure 3a), and the results accord with the

known lattice spacing for bulk Fe₃O₄ along with their respective hkl indexes from the PDF database. The high-resolution transmission electron micrograph (HRTEM) of a single Fe₃O₄ NP with diameter of 14 nm shown in Figure 3b illustrates the highly crystalline nature of the Fe₃O₄ NPs.

The highly ordered arrays of the Fe₃O₄ nanocrystals are formed by slow evaporation of the heptane solution of Fe₃O₄ NPs on Formvar-coated copper grids. When dilute dispersion (with concentration of 0.005 mole per liter) of the Fe₃O₄ NPs is deposited onto the substrate, monodisperse Fe₃O₄ NPs are self-assembled (SA) into the ordered monolayer as shown in Figure 3c. Higher initial concentration (with concentration of 0.02 mole per liter) of the Fe₃O₄ NPs solution leads to the superlattice formation of multilayers as shown in Figure 3d. The superlattice formations of the Fe₃O₄ NPs are driven by surface tension, attractive van der Waals forces, and magnetic interaction among the superparamagnetic nanoparticles.⁶ Figure 3d shows that the Fe₃O₄ NPs are self-assembled in a hexagonal closed packed way, which demonstrates, on the other hand, the uniformity of the particles' sizes, which is necessary for the ordered structure and is necessary for application and fundamental investigation purpose. In Figure 3c and d, the Fourier transform power spectra (FFT) of the ordered structure of Fe₃O₄ NPs confirm the hexagonal symmetry. By adjusting the evaporation temperature to about 35 °C, one can get superlattices with large areas. Figure 3e shows the TEM image of the superlattice with ordered area extending over 0.8 $\mu\text{m} \times 0.7 \mu\text{m}$. The average size of NPs in Figure 3e is 4.0 ± 0.25 nm, and the standard deviation about the mean size is about 4% (400 nanoparticles were measured).

The magnetic properties of monodisperse Fe₃O₄ NPs with diameter of 8 nm in different physical states were investigated using a physical properties measurement system (PPMS). The temperature dependence of magnetization was measured at an applied field of 300 Oe between 5 and 300 K using the zero-field-cooling (ZFC) and field-cooling (FC) procedures. The hysteresis loops were measured at 10 and 300 K, respectively. The sample in the powder state is named sample 1, and the ones diluted with wax with concentration of 1.15% and 0.49% in the mass are named sample 2 and sample 3, respectively. The FC and ZFC curves of the three samples are shown in Figure 4a,b. One can see that all the FC and ZFC curves exhibit

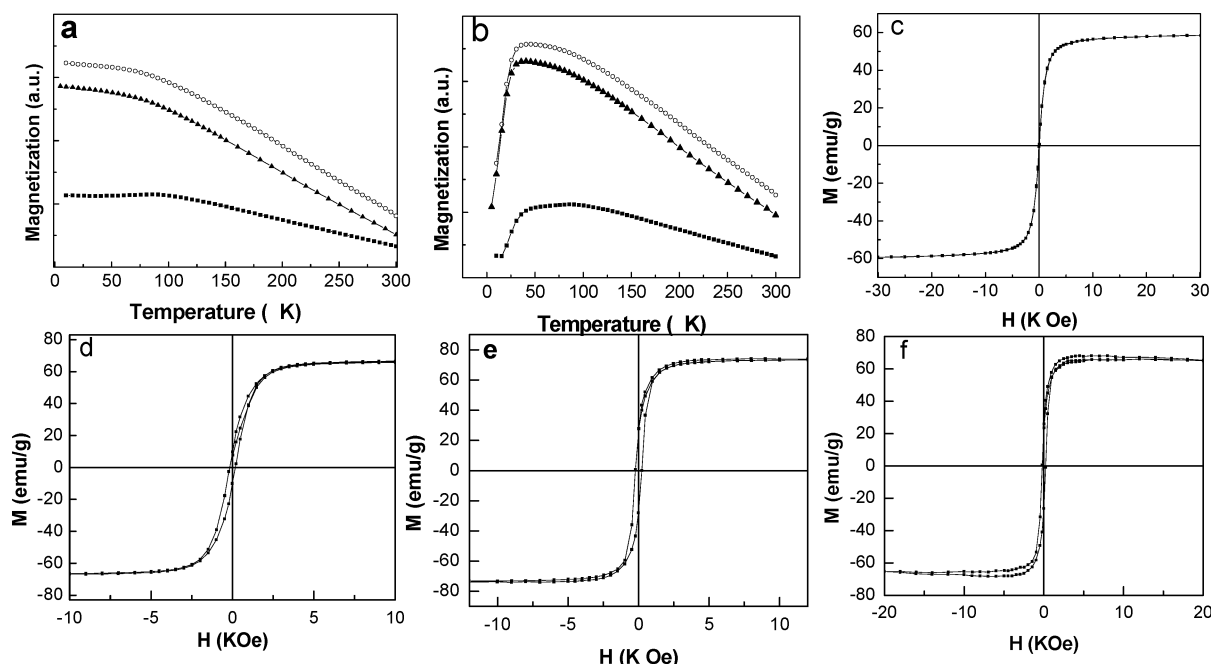


Figure 4. (a, b). Magnetization as a function of temperature, measured in FC case (a) and in ZFC case (b). In both (a) and (b), the solid squares form the curve of sample 1, the open circles constitute the curve of sample 2, and the solid triangles constitute the curve from sample 3. (c, d). Hysteresis loop measured at 300 K (c) and 10 K (d) for 8 nm NPs in powder state. (e, f). Hysteresis loop measured at 10 K for 8 nm magnetite NPs diluted with wax; the concentration in mass is 1.15% (e) and 0.49% (f).

TABLE 2: Magnetic Properties of Fe₃O₄ NPs in Different Physical States^a

	M_s (300 K) emu/g	M_s (10 K) emu/g	M_r emu/g	M_r/M_s	H_c Oe	FC slope 150–300 K emu/(gK)	ZFC slope 150–300 K emu/(gK)
sample 1	58.94	67.04	7.41	0.11	160.1	0.04	0.04
sample 2	64.41	73.45	26.78	0.36	230.6	0.11	0.11
sample 3	57.38	64.92	23.94	0.37	241.8	0.10	0.10

^a H_c , M_r , and M_r/M_s are enhanced by increasing the interparticle distances.

similar behaviors (especially sample 2 and sample 3) at high temperature above the blocking temperature (T_B), which is about 40 K here, and which indicates the particles are free to align with the field during the measuring time at high temperature. This state is considered to be superparamagnetic, because the particles behave similarly to paramagnetic materials but with a much larger moment. All the curves show that the magnetization decreases with temperature linearly above the T_B . And, it is in agreement with the Curie–Weiss law to some extent. The only difference between them is in the slopes (see Table 2). The slopes of the same sample in both ZFC and FC measurement are equal to each other, but those from samples 2 and 3 are much bigger than those from sample 1. It may be caused by the increasing interplay among the particles, which affects the interparticle exchange interaction, and further investigation may introduce some new parameters, such as interparticle distances, into the Curie–Weiss law when it is used at the nanometer scale.

Below the T_B , the ZFC curves show a gradual increase of the magnetization with temperature up to around 41 K, which suggests progressive rotation of the magnetization of the blocked magnetic particles toward the field direction. In other words, bigger and bigger particles unfroze their moments. At the blocking temperature, the magnetization reaches the maximum. While at low temperature below the T_B , the FC curves decreases slightly and plateaus finally (sample 1) or increases slowly (samples 2 and 3). In our opinion, the exchange interaction between the atoms of neighboring particles at the surface and the interplay between the NPs lead to the difference between sample 1 and samples 2 and 3. The different behavior of the

curves between ZFC and FC is probably caused by the following facts: The ZFC magnetization is given by the net projection along the H (outer field) of the randomly frozen magnetic moment of the particles with larger radius and of the polarized superparamagnetic NPs, while the FC magnetization corresponds to the net projection of the polarized frozen moments and those of polarized superparamagnetic NPs.

Figure 4c,d shows the hysteresis loops of the 8 nm dried Fe₃O₄ powder at 10 and 300 K, respectively. The hysteresis loop (Figure 4c) at room temperature of the dried powder shows the expected behavior. At 300 K, the magnetite nanoparticles do not display magnetic remanence, and the initial slopes of the magnetization curve are steep. These facts are related to finite-size and surface effects. According to this case, the particles are considered to be superparamagnetic. The steep initial slopes show promise for applications in nanoscale magnetic devices. The hysteresis loop of Fe₃O₄ powder shows ferrimagnetic-like properties at 10 K (Figure 4d). The M_s (saturation magnetization) is about 67.04 emu/g, the coercive field H_c is about 160.1 Oe, and the remanent magnetization M_r is about 7.4 emu/g. It is roughly in agreement with the data from the literature.¹⁶ The difference may come from the dipolar interactions among the NPs, the different particle sizes, and the spacing among the particles. The hysteresis loops from samples 2 and 3 at 10 K were shown in Figure 4e and f, respectively, and all the characteristic data are shown in Table 2. One can see that H_c , M_r , and M_r/M_s were enhanced when the NPs were diluted with wax. These enhancements probably originate from the decrease of interparticle exchange interaction caused by the

increasing interplay among the particles and the occurrence of a collective interparticle magnetic state.²⁰ For all the samples, one can see that the M_s at 300 K is smaller than at 10 K. Lower M_s is expected at higher temperature because of the superparamagnetism.

Conclusions

We have obtained magnetite nanoparticles with narrow size distribution. The size can be controlled by varying the experimental parameters. Highly ordered monolayer and multilayer self-assemblies with a large area of the Fe_3O_4 NPs have been obtained, which is so important in respect to the applications. The magnetite NPs are ferrimagnetic at 10 K, while at room temperature, it is superparamagnetic. The H_c , M_r , M_r/M_s , and the slopes of the FC/ZFC at high temperature of the NPs were enhanced by diluting them with wax. It has also been seen that different temperature leads to different saturation magnetization. The unique properties caused by surface and finite-size effects suggest a promising future of the NPs in practical applications.

Acknowledgment. We are much obliged to M. Dotson for the helpful discussion and critical reading of the manuscript. The project is supported by the National Nature Science Foundation of China, National “863” and “973” project of China, the Chinese Academy of Sciences, and “key technologies research and development program” of China.

References and Notes

- (1) Dai, S.; Burleigh, M. C.; Ju, Y. H.; Gao, H. J.; Lin, J. S.; Pennycook, S. J.; Barnes, C. E.; Xue, Z. L. *J. Am. Chem. Soc.* **2000**, *122*, 992.
- (2) Bosman, A. W.; Janssen, H. M.; Meijer, E. W. *Chem. Rev.* **1999**, *99*, 1665.
- (3) Shen, C. M.; Su, Y. K.; Yang, H. T.; Yang, T. Z.; Gao, H. J. *Chem. Phys. Lett.* **2003**, *373*, 39.
- (4) Steigerwald, M. L.; Brus, L. E. *Acc. Chem. Res.* **1990**, *23*, 183.
- (5) Yang, H. T.; Shen, C. M.; Su, Y. K.; Yang, T. Z.; Gao, H. J. *Appl. Phys. Lett.* **2003**, *82*, 4729.
- (6) Puentes, V. F.; Krishnan, K. M.; Alivisatos, P. *Appl. Phys. Lett.* **2001**, *78*, 2187.
- (7) Moralesy, M. P.; Sernaz, C. J.; Bødkerx, F.; Mørupx, S. *J. Phys.: Condens. Matter.* **1997**, *9*, 5461.
- (8) Kim, D. K.; Mikhaylova, M.; Wang, F. H.; Kehr, J.; Bjelke, B.; Zhang, Y.; Tsakalakos, T.; Muhammed, M. *Chem. Mater.* **2003**, *15*, 4343.
- (9) Woo, K. G.; Hong, J. W.; Choi, S. M.; Lee, H. W.; Ahn, J. P.; Kim, C. S.; Lee, S. W. *Chem. Mater.* **2004**, *16*, 2814.
- (10) Johnson, B. K.; Prud'homme, R. K. *Phys. Rev. Lett.* **2003**, *91*, 118302.
- (11) Mallinson, J. C. *The Foundations of Magnetic Recording*; Academic: Berkeley, 1987; Chapter 3.
- (12) Bradley, F. N. *Materials for Magnetic Functions*; Hayden: New York, 1976; Chapter 2.
- (13) Willner, I.; Patolsky, F.; Wasserman, J. *Angew. Chem., Int. Ed.* **2001**, *40*, 1861.
- (14) Maoz, R.; Frydman, E.; Cohen, S. R.; Sagiv, J. *Adv. Mater.* **2000**, *12*, 424.
- (15) Stephen, F.; Hakan, R.; Nagaraja, R. S.; Donald, F. *Chem. Mater.* **2002**, *14*, 3643.
- (16) Sun, S. H.; Zeng, H.; Robinson, D. B.; Raoux, S.; Rice, P. M.; Wang, S. X.; Li, G. X. *J. Am. Chem. Soc.* **2004**, *126*, 273.
- (17) Kim, T. Y.; Lee, M. S.; Kim, Y. I.; Lee, C. S.; Park, J. C.; Kim, D. *J. Phys. D: Appl. Phys.* **2003**, *36*, 1451.
- (18) Harris, L. A.; Goff, J. D.; Carmichael, A. Y.; Riffle, J. S.; Harburn, J. J.; St. Pierre, T. G.; Saunders, M. *Chem. Mater.* **2003**, *15*, 1367.
- (19) Moudler, J. F.; Stickle, W. F.; Sobol, P. E.; Bonben, K. D. *Handbook of X-ray photoelectron spectroscopy*; Perkin-Elmer: Eden Prairie, MN, 1992.
- (20) Zysler, R. D.; Fiorani, D.; Testa, A. M. *J. Magn. Magn. Mater.* **2001**, *224*, 5.